HHS Public Access

Author manuscript

Nucl Med Biol. Author manuscript; available in PMC 2021 July 01.

Published in final edited form as:

Nucl Med Biol. 2020 ; 86-87: 1–8. doi:10.1016/j.nucmedbio.2020.04.002.

Biodistribution, dosimetry, and temporal signal-to-noise ratio analyses of normal and cancer uptake of [^{68}Ga]Ga-P15-041, a gallium-68 labeled bisphosphonate, from first-in-human studies

Robert K. Doot[1], **Anthony J. Young**[1], **Margaret E. Daube-Witherspoon**[1], **David Alexoff**[2], **Kyle J. Labban**[1], **Hwan Lee**[1], **Zehui Wu**[2], **Zhihao Zha**[2], **Seok R. Choi**[2], **Karl H. Ploessl**[2], **Erin K. Schubert**[1], **Hsiaoju Lee**[1], **Lin Zhu**[2], **Janet S. Reddin**[1], **Joel S. Karp**[1], **Hank Kung**[2], **Daniel A. Pryma**[1]

[1]Department of Radiology, University of Pennsylvania

[2]Five Eleven Pharma Inc., Philadelphia, PA 19104

Abstract

Introduction: [^{68}Ga]Ga-P15-041 ([^{68}Ga]Ga-HBED-CC-BP) is a novel bone-seeking PET radiotracer that can be generator-produced. We undertook a Phase 0/I clinical trial to assess its potential for imaging bone metastases in prostate cancer including assessment of radiotracer biodistribution and dosimetry.

Methods: Subjects with prostate cancer and known or suspected osseous metastatic disease were enrolled into one of two arms: dosimetry or dynamic. Dosimetry was performed with 6 whole body PET acquisitions and urine collection spanning 3 hours; normal organ dosimetry was calculated using OLINDA/EXM. Dynamic imaging included a 60-minute acquisition over a site of known or suspected disease followed by two whole body scans. Bootstrapping and subsampling of the acquired list-mode data were conducted to recommend image acquisition parameters for future clinical trials.

Results: Up to 233 MBq (6.3 mCi) of [^{68}Ga]Ga-P15-041 was injected into 12 enrolled volunteers, 8 in dosimetry and 4 in dynamic cohorts. Radiotracer accumulated in known bone lesions and cleared rapidly from blood and soft tissue. The highest individual organ dose was 0.135 mSv/MBq in the urinary bladder wall. The average effective dose was 0.0173 ± 0.0036 mSv/MBq. An average injected activity of 166.5 MBq (4.5 mCi) resulted in absorbed dose

Corresponding author: Robert K. Doot, PhD, University of Pennsylvania, John Morgan Building, room 160A, 3620 Hamilton Walk FL 1, Philadelphia, PA 19104-4800, Phone: (215) 573-6016, Fax: (215) 573-3880, robdoot@pennmedicine.upenn.edu.

Conflicts of Interest

Authors David Alexoff, Zehui Wu, Zhihao Zha, Seok Choi, Karl Ploessl, Lin Zhu, and Hank Kung are employees of Five Eleven Pharma, which holds the patent rights for [^{68}Ga]Ga-P15-041 [34] and related technology. Daniel Pryma is a member of the Scientific Advisory Board for Five Eleven Pharma.

Data Statement

The informed consent obtained from participants prior to data collection did not include permission to share data with outside investigators and therefore we cannot share the supporting data.

estimates of 22.5 mSv to the urinary bladder wall, 8.2 mSv to the kidneys, and an effective dose of 2.9 mSv. Lesion signal to noise ratios on images generated from subsampled data were significantly higher for injected activities above 74 MBq (2 mCi) and were also significantly higher for imaging at 90 minutes than at 180 minutes post-injection.

Conclusions: Dosimetry estimates are acceptable and [^{68}Ga]Ga-P15-041 uptake characteristics in patients with confirmed bone metastases support its continued development.

Advances in Knowledge and Implications for patient care: Use of [^{68}Ga]Ga-P15-041 would not require cyclotron infrastructure for manufacturing and distribution, allowing for improved patient access to a promising PET bone imaging agent.

Keywords

PET; bisphosphonate; prostate cancer; bone metastases; Gallium-68

1. Introduction

Prostate cancer is the most common non-cutaneous malignancy among US men and is the second leading cause of cancer death. In 2019, approximately 174,650 men will be diagnosed with prostate cancer and approximately 31,620 will die from it [1]. It is estimated that the disease will affect one in nine men in their lifetimes [1]. Bone metastases are the defining feature of advanced prostate cancer and imaging is an important clinical tool in the diagnosis, staging, and evaluation of metastases in patients with prostate cancer. [^{68}Ga]Ga-P15-041 is a novel bone-seeking Positron Emission Tomography (PET) radiotracer with generator production capability, which enables bone PET/Computed Tomography (CT) imaging without a cyclotron. We undertook a Phase 0/I clinical trial to evaluate its use for imaging bone metastases in prostate cancer.

Bisphosphonates (BPs), shown in Figure 1, have been widely used to treat osteoporosis and bone metastases by binding to bone mineral to inhibit the resorptive function of osteoclasts. They provide generally safe and effective osteoporosis treatment in humans [2, 3]. Methylene diphosphonate (MDP) labeled with technetium-99m is a BP without sidechains that is one of the most commonly used radiopharmaceutical imaging agents over the past forty years [4]. Bone scintigraphy using [^{99m}Tc]Tc-MDP is very useful in the evaluation of bone disorders, such as infection (osteomyelitis), noninfectious inflammation (arthritis), trauma, metabolic bone disease, benign and malignant neoplasms, and metastasis. Nevertheless, there are concerns about recurring shortages of technetium-99m supply, which may limit the availability of this imaging agent for routine clinical use. Furthermore, tomographic imaging of the PET radiotracer [^{18}F]fluoride has been shown to be superior to bone planar scintigraphy and SPECT/CT using [^{99m}Tc]Tc-MDP [5]. This suggests an alternative BP bone binding PET radiotracer to [^{99m}Tc]Tc-MDP and sodium [^{18}F]fluoride would be clinically useful.

^{68}Ge/^{68}Ga generators for PET imaging are becoming increasingly available [6, 7]. A long-lived parent isotope, germanium-68 ($t_{1/2}$ 271 d), allows for easy and widespread generator distribution [7–10], providing a convenient mechanism for positron emitting isotope

production without the need for a nearby cyclotron. Furthermore, the physical properties of the daughter gallium-68 ($t_{1/2}$ 68 min, 89% β^+) are highly suitable for PET imaging, though its positron energy (E_{max} 1.92 MeV) is higher than ideal.

A large number of gallium-68 complexes have been reported. They are usually metal-chelating macrocyclic or acyclic polyaza carboxylic acids designed originally to form gadolinium complexes for use as magnetic resonance imaging (MRI) contrast agents, such as: diethylenetriaminepentaacetic acid [11], 1,4,7,10-tetraazacyclododecane-1,4,7,10-tetraacetic acid (DOTA), 1,4,7-triazacyclononane-1,4,7-triacetic acid (NOTA), and other polycyclic derivatives. By using DOTA and NOTA derivatives, many gallium-68 labeled bisphosphonates were prepared and tested for bone imaging [12–17]. It was reported that a bisphosphonate DOTA derivative, [^{68}Ga]Ga-4-[[(bis-phosphonomethyl) carbomoyl]methyl]-7,10-bis-(carboxymethyl)-1,4,7,10-tetraazacyclododec-1-yl)-acetic acid (BPAMD) [14, 16, 18], displayed good bone uptake and retention in humans. The DOTA and NOTA based bisphosphonates, gallium-68 labeled BPAMD [16] and NO2APBP [13], have also been successfully tested in humans as bone-imaging agents. Most recently, [^{68}Ga]Ga-DOTA^{ZOL}, a DOTA based bisphosphonate based on the therapeutic drug zoledronate, was evaluated in an early phase human trial and showed promising preliminary results [19].

In developing the novel radiotracer being tested for this study we used the core ligand N, N'-bis(2-hydroxybenzyl)ethylenediamine-N,N'-diacetic acid (HBED), which is known as a metal chelating agent for In^{3+}, Fe^{3+} and Ga^{3+} first reported a few decades ago [20, 21]. The human experience of Fe-HBED (Figure 1) was associated with the removal of excess iron in the blood as a potential alternative to deferoxamine for treatment of chronic iron overload and acute iron poisoning. The HBED chelating group used in P15-041 for Ga^{3+} is well known, and results from a Phase I clinical trial suggested relatively low toxicity for this chelating group [22, 23]. In this project, HBED was used instead of commonly employed DOTA and NOTA as the core ligand for chelating Ga^{3+} because the stability constants (log K_d) for Ga^{3+}-DOTA and Ga^{3+}-NOTA complexes (log K_d = 26.05 and 29.63, respectively) were less compared to Ga^{3+}-HBED, which forms a stronger, more stable Ga^{3+} complex (log K_d = 39.57) [11, 24–26]. Additionally, literature shows that HBED out complexes DOTA and NOTA by 99% and 43%, respectively during competition studies with equimolar amounts of ligands with gallium [26]. This indicates that the kinetic and thermodynamic stability of gallium-68 HBED complexes are greater than [^{68}Ga]Ga-DOTA or [^{68}Ga]Ga-NOTA complexes. It implies that a kit formulation and mild reaction conditions would be more suitable with HBED compared to DOTA and NOTA ligands. Based on the success of [^{68}Ga]Ga-Glu-NH-CO-NH-Lys(Ahx)-HBED-CC as a PSMA-targeting imaging agent in humans [27–32], an HBED-CC derivative containing bisphosphonates, [^{68}Ga]Ga-P15-041, was prepared as shown in Figure 1.

We hypothesize that the gallium-68 chelating part of the molecule, HBED-CC, is not likely to interfere with the bone-targeting bisphosphonate group. This new compound, therefore, contains two independent components. First, the HBED chelating group is designed to form a stable complex with [^{68}Ga]Ga^{3+} as indicated above; second, the bisphosphonate group attached at the end of the chelating group is utilized for targeting and binding to

hydroxyapatite on active bone surfaces, similar to the phosphonate group of [^{99m}Tc]Tc-MDP. In our preclinical work [^{68}Ga]Ga-P15-041 showed excellent bone uptake in normal CD-1 IGS male mice and in comparison with [^{68}Ga]Ga-BPAMD it showed twice the retention at 60 min and had a similar value to [^{18}F]fluoride (23.5 vs 9.2% injected activity/g for [^{68}Ga]Ga-P15-041 and [^{68}Ga]Ga-BPAMD, respectively, and 24.2% injected activity/g for [^{18}F]fluoride under comparable conditions) [33]. The purpose of this study was to evaluate the biodistribution and dynamic uptake resulting from administration of [^{68}Ga]Ga-P15-041 in human males with confirmed prostate cancer and determine its feasibility for use as a bone metastasis imaging agent.

2. Methods

2.1 Volunteers

This study was conducted in accordance with the Declaration of Helsinki, and the University of Pennsylvania Institutional Review Board (FWA00004028) approved all procedures and the ClinicalTrials.gov Identifier is NCT02826382. Informed consent was obtained from all subjects who participated in the study. Male volunteers 18 years and older with prostate cancer and known or suspected osseous metastatic disease who were referred for a clinical [^{99m}Tc]Tc-MDP bone scan were eligible for enrollment into either the dosimetry or dynamic cohort.

2.2 Radiochemistry

The [^{68}Ga]Ga-P15-041 radiopharmaceutical, also known as [^{68}Ga]Ga-3-(3-(((carboxymethyl)(2-((carboxymethyl)(5-(3-((diphosphonomethyl)amino)-3-oxopropyl)-2-hydroxybenzyl)amino)ethyl)amino)methyl)-4-hydroxyphenyl)propanoic acid, was prepared using an automated radiolabeling and purification system designed for gallium-68 drug preparation by Five Eleven Pharma Inc. [34] in combination with [^{68}Ga]Ga^{3+} from a ^{68}Ge/^{68}Ga generator 1.11 GBq (30 mCi) produced by ITG (Isotope Technologies, Garching GmbH) under Investigational New Drug (IND) # 129870. Briefly, the automated system's syringe pump was used to elute the generator with 4 mL of 0.05 M HCl at a flow rate of ~ 2 mL/min, delivering the eluate directly into a septum-capped vial containing P15-041 (~ 29 microgram) and NaOAc•3H_2O (68 mg) as a lyophilized powder. The reaction mixture was heated for 5 min at 70 °C, cooled for ~ 30 s using a fan and then diluted with 3 mL of sterile water. The [^{68}Ga]Ga-P15-041 product was isolated on a Sep Pak™ Plus Light aminopropyl cartridge (Waters Corporation, Milford, Massachusetts) used as a weak anion exchanger, previously conditioned with ethanol followed by 0.05 N HCl. The trapped [^{68}Ga]Ga-P15-041 was rinsed with 4 mL of sterile water then recovered by eluting the Sep Pak™ with 2 mL of 0.1 N NaOH. The eluate was delivered directly into a vial previously loaded with HCl (1.0 mL 0.2 N), sterile saline (6 mL) and NaOAc,3H_2O (32 mg). The resulting pH-adjusted solution (9 mL) was passed through a 25 mm sterile vented 0.2 μm MCE filter (Millex-GS) into a sterile septum-capped final product vial. Final product pre-release quality control procedures were: visual inspection of the final product vial solution; pH measurement; radiochemical purity determination by iTLC; half-life determination to confirm radionuclidic identity; endotoxin testing (Endosafe™ PTS, Charles River Laboratories, Charleston, South Carolina); and a bubble point determination to confirm the

integrity of the filter used for sterilization by terminal filtration. Product sterility was validated post-release for each batch.

For iTLC a mixture of 0.2 N NaOAc, acetone and acetyl acetone (6.7:60:33.3 v/v) was used as mobile phase and a cellulose TLC plate was used for separation. If present, unlabeled gallium-68 will move with the solvent front with an R_f approximately equal to 1. [^{68}Ga]Ga-P15-041 is expected to have an R_f value ≤ 0.1. The germanium-68 content in the final product from generator germanium-68 breakthrough was measured during a validation run that was carried out for each new generator. Briefly, a production run was performed as described above and activity in the final product vial (~8.5 mL) was assayed immediately after production (EOS) in an ion chamber, and then again in a NaI-crystal well-type counter after at least 3 days of decay and after ~ 1 mL aliquot for pre-release QC was removed. The ion chamber and well-type counter were cross calibrated using standard procedures, and the ratio of the activity concentration after 3 days to the EOS activity concentration was calculated and compared to IND specifications. The same methods were used to measure generator germanium-68 breakthrough of the gallium-68 eluate (4 mL 0.05 N HCl). After validation, generator germanium-68 breakthrough in a maintenance rinse was typically determined weekly to assure that the final product germanium-68 content met IND specifications.

2.3 Dosimetry cohort imaging

Eight male subjects enrolled in the dosimetry cohort had confirmed prostate cancer with known or suspected osseous metastatic disease. All eight underwent 6 PET whole body scans using a Philips Ingenuity PET/CT scanner (Philips Healthcare, Andover, MA, USA) over approximately 3 hours following the intravenous administration of [^{68}Ga]Ga-P15-041. Two low dose CT scans were used for attenuation correction of the 6 PET scans with the first and second low dose CT scans allowing attenuation correction of the first 4 and last 2 PET scans, respectively. The use of a second low dose CT attenuation scan allowed volunteers to leave the PET/CT scanner between PET scans 4 and 5 to void their bladders. The PET scanner has a 70-cm diameter gantry opening, an 18-cm axial FOV, and a PET spatial resolution of 4.8 mm full width at half maximum, sensitivity of 7.3 cps/kBq, and peak trues rate of 365 kcps [35]. Top of skull to mid-thigh whole body PET scans were acquired over 15 minutes in 10 bed positions with 90 s per bed position with about 50% bed overlap; acquisitions started at approximately 1, 20, 40, 60, 120, and 150 min after radiotracer injection. Subjects had opportunities to void their bladders after the fourth and sixth PET/CT scans and urine was collected separately for each void. Activity concentrations in urine samples were assessed via a 2480 WIZARD^2 automatic gamma counter (PerkinElmer, Waltham, MA, USA). Total activity residing in brain, heart contents, intestines, kidneys, liver, lungs, spleen, and urinary bladder were measured directly from PET images via Pmod v3.7 software (Pmod Technologies LLC, Zurich, Switzerland). Activity in approximately 5 cm of each femur shaft was measured and used to estimate total activity uptake in cortical bone at each time point. The total activity residing in cortical bone was estimated by multiplying the mean cortical bone count density by the mean volume of cortical bone in adult males of 2130 cm^3 [36]. Time activity curves for source organs were generated and, in most cases, the curves were fit to mono- or bi-exponential functions using

OLINDA | EXM v1.1 software [37]. For time activity curves that were poorly fit by exponential functions, a Riemann Sum was used to calculate numbers of disintegrations occurring in organs. Dosimetry estimates were calculated using the Standard Adult Male phantom in OLINDA | EXM v1.1 software.

2.4 Dynamic cohort imaging

Five subjects with confirmed prostate cancer with known or suspected osseous metastatic disease underwent both a [^{99m}Tc]Tc-MDP planar bone scintigraphy started approximately 3 hours post-injection with a duration of about 24 minutes and a 60-minute dynamic PET acquisition from time of injection over a site of known or suspected disease. Imaging results for one of subjects was excluded from analyses since his PET acquisition was terminated after 27 minutes due to discomfort unrelated to the scan. Whole body PET/CT scans from skull-base to mid-thigh were then conducted at approximately 90 and 180 minutes post injection. Image analyses were performed using Pmod v3.7 software. Peak standardized uptake values (SUVp) were determined according to Wahl [38] and Vanderhoek [39] using a 1 cm diameter sphere located on bone lesions, blood pool, and normal bone. Time activity curve results from Pmod software were analyzed in Microsoft Excel version 15 (Microsoft, Redmond WA, USA) and plotted using Prism 7 software (GraphPad Software, Inc., La Jolla, CA, USA).

2.5 Subsampling of PET images

Subsamples of the acquired list-mode data to emulate lower injected activities were analyzed to guide recommendations on PET image acquisition protocol parameters (injected activity and injection-to-scan-start interval). Subsampled PET data were reconstructed with a clinical list-mode TOF ordered subsets expectation maximization algorithm [35] into 4-mm voxels. Uptake measurement precision was assessed using ten replicate datasets generated by bootstrapping the original list-mode data [40, 41]. Subsampling of the data was performed to emulate lower injected activities of 74, and 37 MBq by reconstructing corresponding fractions of the events in the original data [42]. Lesion maximum uptake (L_{max}) was measured in 4 to 11 regions of focal bone uptake in each subject, and the standard deviation (SD) across the 10 replicate datasets and signal-to-noise ratio (SNR), calculated as the L_{max} divided by the L_{max} SD, were determined for each lesion at each injection-to-scan-start interval and activity level. In addition, the change in uptake with scan interval post-injection, which may reflect the change in physiological uptake in the lesions, was calculated after decay correction.

2.6 Statistics

Statistical analyses were performed using IBM SPSS 25 (IBM Armonk, NY, USA) and included comparisons between lesion SD and signal to noise across emulated activity for bootstrapped replicates using one-way repeated measures MANOVA (alpha < 0.05) with post-hoc comparisons of marginal means Bonferroni adjusted for multiple comparisons. Comparisons of lesion uptake, SD, and SNR between 90 and 180-minute post-injection scans were performed using two-tailed paired t-tests (alpha < 0.05). Additionally, for patients with dynamic imaging, lesions within the dynamic scan field of view were measured at 60, 90, and 180 minutes, with comparisons of lesion uptake, SD, and SNR

performed using one-way repeated measures MANOVA (alpha < 0.05) with post-hoc analysis corrected for multiple comparisons.

3. Results

Demographic data for subjects are in Table 1.

3.1 Production of [^{68}Ga]Ga-P15-041

Production of the [^{68}Ga]Ga-P15-041 radiopharmaceutical using Five Eleven Pharma's automated system was reliable and yielded a product of high radiochemical purity (98.8% ± 1.70% ; n=13). The decay-corrected yield was estimated to be 85% ± 2.8% (n=11) based on the assumption that the starting activity was equal to the gallium-68 activity measured in a recent generator maintenance rinse. Automated production time was 16 min.

3.2 Subject tolerability to [^{68}Ga]Ga-P15-041 administration

[^{68}Ga]Ga-P15-041 was administered to 13 subjects (12 completed protocol) and was well-tolerated with no reports of serious adverse events. Three patients reported a Grade 1 adverse event (per National Cancer Institute's Common Terminology Criteria for Adverse Events v 4.0) including nausea and/or diarrhea. For two of the 3 reporting subjects, the events were attributed to recent treatment / chemotherapy and judged to be unrelated to [^{68}Ga]Ga-P15-041 administration. In one subject with diarrhea the event causality was judged unlikely related. No clinically significant changes were noted between vital signs collected before and after injection of the radiotracer.

3.3 Dosimetry cohort

Eight adult male volunteers (ages 59-73, mean 68 years old) were enrolled into the dosimetry cohort and injected with [^{68}Ga]Ga-P15-041 at a mean activity of 165 MBq, range 86-232 MBq (4.5 mCi, 2.3-6.3 mCi). The [^{68}Ga]Ga-P15-041 average absorbed dose estimates for the eight dosimetry cohort volunteers are in Table 2. An example of the biodistribution of [^{68}Ga]Ga-P15-041 as a function of time after radiotracer injection is shown by the PET maximum-intensity projections in Figure 2. Mean [^{68}Ga]Ga-P15-041 injected activity percentages in organs as functions of time are in Figure 3. The highest individual organ dose was 0.135 mSv/MBq in the urinary bladder wall. The average effective dose was 0.0173 ± 0.0036 mSv/MBq. An injected activity of 166.5 MBq (4.5 mCi) of [^{68}Ga]Ga-P15-041 resulted in doses of 22.5 mSv to the urinary bladder wall, 8.2 mSv to the kidneys, and an effective dose of 2.9 mSv.

3.4. Dynamic cohort

The four male volunteers enrolled into the dynamic cohort that completed all PET/CT scans had a mean [^{68}Ga]Ga-P15-041 injected activity of 149 MBq (range 115 to 193 MBq) and a mean [^{99m}Tc]Tc-MDP injected activity of 1020 MBq (range 977 to 1080 MBq). Representative [^{68}Ga]Ga-P15-041 PET and [^{99m}Tc]Tc-MDP planar bone scintigraphy images of osseous metastases in the same patient are displayed in Figure 4. As expected the PET images have higher contrast with more detectable lesions than the planar bone images. Figure 5 shows time activity curves for the highest uptake metastases, average blood pool,

and mean normal bone. Activity concentrations of [^{68}Ga]Ga-P15-041 in blood and normal bone (Figure 5) were low compared to sites of osseous metastasis and relatively constant at later time points, while individual tumor activity concentrations usually continued to increase over time.

3.5. Subsampled dynamic cohort PET images

The four acquired PET image sets from the dynamic cohort were subsequently subsampled to emulate the impact of lower injected activities of radiotracer to inform selection of image acquisition parameters for future clinical trials. The resulting average percent standard deviation (%SD) of lesion max uptake (L_{max}) across the 10 bootstrapped replicates is plotted as a function of emulated injected activity in Figure 6A. Average lesion signal to noise ratio (SNR) was calculated as L_{max} over SD of L_{max} to determine the signal strength as shown in Figure 6B.

The impact of the injection-to-scan-start interval was analyzed using L_{max}, %SD, and SNR for each lesion. Scanning beyond 90 minutes resulted in increased lesion uptake ($p<0.001$), but with a corresponding increase in %SD ($p<0.001$). Thus, SNR varied with injection-to-scan-start interval, decreasing between 90 and 180 minutes across all patients and lesions ($p<0.001$, Figure 7). A total of 8 lesions in the 4 patients with dynamic imaging showed no significant difference in lesion uptake between the 60-minute image and the 90 and 180-minute static scans (L_{max} $p = 1$, %SD $p \geq 0.43$, and SNR $p \geq 0.66$).

Subsampled images at lower emulated activities were compared to original injected activities using %SD and SNR. As seen in Figure 6, lesion %SD decreases and SNR increases with increasing emulated activities of 37-117 MBq (1-3.2 mCi); changes in %SD and SNR were significant ($p<0.05$ and $p<0.003$, respectively). At subsampled activities of 111 MBq (3 mCi) and above, lesion %SD and SNR across the bootstrapped replicates were similar to original injected activities, (n=2 patients, 15 total lesions, $p=1$ for both %SD and SNR). The subsampled PET images to emulate lower injected activities results are consistent with improved lesion detection at activities above 74 MBq, but with little difference in quantitation between activities at or above 111 MBq.

4. Discussion

Radiopharmaceutical bone imaging remains a critical component of nuclear medicine with considerable impact in the care of patients with prostate cancer and other diseases. Bone imaging with PET/CT has been shown to be superior to both planar and SPECT/CT bone scintigraphy [5], but imaging with sodium [^{18}F]fluoride is limited by the need for a cyclotron as well as the lack of a blood pool phase for three phase imaging. A gallium-68 based PET bone radiopharmaceutical can address both of these limitations. Earlier generation agents had acceptable biodistributions but employ the DOTA or NOTA chelators, which are known to have lower Ga^{3+}-chelator complex stability constants compared to Ga^{3+}-HBED [11, 24–26]. [^{68}Ga]Ga-P15-041 was designed in part to test whether a higher Ga^{3+}-complex stability could lead to an improved gallium-68 based PET bone imaging agent. Promising preclinical testing including in-vivo stability and pharmacokinetic

measurements suggested the potential superiority of [^{68}Ga]Ga-P15-041, which led to this study.

We have shown acceptable dosimetry using this agent (2.9 mSv effective dose) as compared to typical adult effective doses of 3.0 mSv for [^{99m}Tc]Tc-MDP [43] and 3.4 mSv for sodium [^{18}F]fluoride [43] with high target to background in sites of bone metastatic disease. Not surprisingly, signal to noise improved with increasing administered activity (Figure 6B), but lower activity emulations show acceptable image quality at activities at and above 111 MBq (3 mCi), permitting potential quality imaging at very low radiation dose in patients with benign disease. Additionally, imaging beyond 60 minutes was not shown to improve lesion uptake quantitation, representing a potential clinical improvement over conventional bone scintigraphy that requires an approximately 3 hour delay between injection and imaging. These encouraging results justify further development of [^{68}Ga]Ga-P15-041 including testing performance in other common clinical indications for [^{99m}Tc]Tc-MDP bone scintigraphy such as suspected osteomyelitis, occult bone fractures, bone pain that is otherwise unexplained, and Paget disease [44].

5. Conclusions

Metastatic prostate cancer lesions were successfully imaged with [^{68}Ga]Ga-P15-041 PET/CT, with lesion uptake consistently above background. Dosimetry results confirm expectations that biodistribution and levels of absorbed doses are adequately low to continue researching [^{68}Ga]Ga-P15-041 radiotracer uptake in humans. Dynamic image analyses of [^{68}Ga]Ga-P15-041 uptake suggests improving signal relative to a constant background over time for the highest uptake tumors, but the SNR analyses suggest imaging between 60 and 90 minutes post-injection to be optimal. The dynamic and dosimetry analyses suggest imaging of prostate bone metastases in humans with [^{68}Ga]Ga-P15-041 PET scans is feasible, but further study with larger cohorts is needed to confirm these early results.

Acknowledgments

The authors thank Joshua S. Scheuermann and Matthew A. Fillare for helpful discussions. Five Eleven Pharma, Inc. was the sponsor of this clinical trial. Research reported in this publication was supported by the United States of America's National Cancer Institute of the National Institutes of Health under award numbers R01CA113941 and R43CA221580 ([^{68}Ga]Ga-P15-041). Development of Five Eleven Pharma's automated synthesis unit is supported by NIH/NCI SBIR award R43CA217425.

References

[1]. Siegel RL, Miller KD, and Jemal A. Cancer statistics, 2019. CA Cancer J Clin 2019;69:7–34. [PubMed: 30620402]

[2]. Lim SY and Bolster MB. Current approaches to osteoporosis treatment. Curr Opin Rheumatol 2015;27:216–24. [PubMed: 25760281]

[3]. McGreevy C and Williams D. Safety of drugs used in the treatment of osteoporosis. Ther Adv Drug Saf 2011;2:159–72. [PubMed: 25083210]

[4]. Jadvar H, Desai B, and Conti PS. Sodium ^{18}F-fluoride PET/CT of bone, joint, and other disorders. Semin Nucl Med 2015;45:58–65. [PubMed: 25475379]

[5]. Schirrmeister H, Glatting G, Hetzel J, Nussle K, Arslandemir C, Buck AK, et al. Prospective evaluation of the clinical value of planar bone scans, SPECT, and ^{18}F-labeled NaF PET in newly diagnosed lung cancer. J Nucl Med 2001;42:1800–4. [PubMed: 11752076]

[6]. Velikyan I Continued rapid growth in ^{68}Ga applications: update 2013 to June 2014. J Label Compd Radiopharm 2015;58:99–121.

[7]. Velikyan I ^{68}Ga-based radiopharmaceuticals: Production and application relationship. Molecules 2015;20:12913–43. [PubMed: 26193247]

[8]. Rosch F, Past, present and future of ^{68}Ge/^{68}Ga generators. Appl Radiat Isot 2013;76:24–30. [PubMed: 23245638]

[9]. Sanchez-Crespo A Comparison of gallium-68 and fluorine-18 imaging characteristics in positron emission tomography. Appl Radiat Isot 2013;76:55–62. [PubMed: 23063597]

[10]. Velikyan I Prospective of ^{68}Ga-radiopharmaceutical development. Theranostics 2013;4:47–80. [PubMed: 24396515]

[11]. Price EW, Zeglis BM, Lewis JS, Adam MJ, and Orvig C. H6phospa-trastuzumab: bifunctional methylenephosphonate-based chelator with ^{89}Zr, ^{111}In and ^{177}Lu. Dalton Trans 2014;43:119–31. [PubMed: 24104523]

[12]. Manzoni L, Belvisi L, Arosio D, Bartolomeo MP, Bianchi A, Brioschi C, et al. Synthesis of Gd and ^{68}Ga complexes in conjugation with a conformationally optimized RGD sequence as potential MRI and PET tumor-imaging probes. ChemMedChem 2012;7:1084–93. [PubMed: 22489059]

[13]. Holub J, Meckel M, Kubicek V, Rosch F, and Hermann P. Gallium(III) complexes of NOTA-bis (phosphonate) conjugates as PET radiotracers for bone imaging. Contrast Media Mol Imaging 2015;10:122–34. [PubMed: 24801892]

[14]. Meckel M, Fellner M, Thieme N, Bergmann R, Kubicek V, and Rosch F. In vivo comparison of DOTA based ^{68}Ga-labelled bisphosphonates for bone imaging in non-tumour models. Nucl Med Biol 2013;40:823–30. [PubMed: 23915801]

[15]. Ogawa K, Takai K, Kanbara H, Kiwada T, Kitamura Y, Shiba K, et al. Preparation and evaluation of a radiogallium complex-conjugated bisphosphonate as a bone scintigraphy agent. Nucl Med Biol 2011;38:631–6. [PubMed: 21718937]

[16]. Fellner M, Baum RP, Kubicek V, Hermann P, Lukes I, Prasad V, et al. PET/CT imaging of osteoblastic bone metastases with ^{68}Ga-bisphosphonates: first human study. Eur J Nucl Med Mol Imaging 2010;37:834. [PubMed: 20069291]

[17]. Suzuki K, Satake M, Suwada J, Oshikiri S, Ashino H, Dozono H, et al. Synthesis and evaluation of a novel ^{68}Ga-chelate-conjugated bisphosphonate as a bone-seeking agent for PET imaging. Nucl Med Biol 2011;38:1011–8. [PubMed: 21982572]

[18]. Fellner M, Biesalski B, Bausbacher N, Kubicek V, Hermann P, Rosch F, et al. ^{68}Ga-BPAMD: PET-imaging of bone metastases with a generator based positron emitter. Nucl Med Biol 2012;39:993–9. [PubMed: 22633217]

[19]. Khawar A, Eppard E, Roesch F, Ahmadzadehfar H, Kurpig S, Meisenheimer M, et al. Preliminary results of biodistribution and dosimetric analysis of [^{68}Ga]Ga-DOTA(ZOL): a new zoledronate-based bisphosphonate for PET/CT diagnosis of bone diseases. Ann Nucl Med 2019;33:404–13. [PubMed: 30877560]

[20]. Motekaitis RJ, Martell AE, and Welch MJ. Stability of trivalent metal complexes of phenolic acids related to N,N′-bis(2-hydroxylbenzyl)-N,N′-diacetic acid (HBED). Inorg Chem 1990;29:1463–7.

[21]. Sun Y, Mathias CJ, Welch MJ, Madsen SL, and Martell AE. Targeting radiopharmaceuticals - II: evaluation of new trivalent metal complexes with different overall charges. Int J Appl Radiat Instrum Part B 1991;18:323–30.

[22]. Grady RW, Salbe AD, Hilgartner MW, and Giardina PJ. Results from a phase I clinical trial of HBED. Adv Exp Med Biol 1994;356:351–9. [PubMed: 7887241]

[23]. Giardina PJ and Grady RW. Chelation therapy in beta-thalassemia: an optimistic update. Semin Hematol 2001;38:360–6. [PubMed: 11605171]

[24]. Motekaitis RJ, Rogers BE, Reichert DE, Martell AE, and Welch MJ. Stability and structure of activated macrocycles. Ligands with biological applications. Inorg Chem 1996;35:3821–7. [PubMed: 11666570]

[25]. Sun Y, Anderson CJ, Pajeau TS, Reichert DE, Hancock RD, Motekaitis RJ, et al. Indium (III) and gallium (III) complexes of bis(aminoethanethiol) ligands with different denticities: stabilities, molecular modeling, and in vivo behavior. J Med Chem 1996;39:458–70. [PubMed: 8558514]

[26]. Tsionou MI, Knapp CE, Foley CA, Munteanu CR, Cakebread A, Imberti C, et al. Comparison of macrocyclic and acyclic chelators for gallium-68 radiolabelling. RSC Adv 2017;7:49586–99. [PubMed: 29308192]

[27]. Afshar-Oromieh A, Haberkorn U, Schlemmer HP, Fenchel M, Eder M, Eisenhut M, et al. Comparison of PET/CT and PET/MRI hybrid systems using a ^{68}Ga-labelled PSMA ligand for the diagnosis of recurrent prostate cancer: initial experience. Eur J Nucl Med Mol Imaging 2014;41:887–97. [PubMed: 24352789]

[28]. Afshar-Oromieh A, Avtzi E, Giesel FL, Holland-Letz T, Linhart HG, Eder M, et al. The diagnostic value of PET/CT imaging with the ^{68}Ga-labelled PSMA ligand HBED-CC in the diagnosis of recurrent prostate cancer. Eur J Nucl Med Mol Imaging 2015;42:197–209. [PubMed: 25411132]

[29]. Chakraborty PS, Tripathi M, Agarwal KK, Kumar R, Vijay MK, and Bal C. Metastatic poorly differentiated prostatic carcinoma with neuroendocrine differentiation: Negative on ^{68}Ga-PSMA PET/CT. Clin Nucl Med 2015;40:e163–6. [PubMed: 25275415]

[30]. Eiber M, Nekolla SG, Maurer T, Weirich G, Wester H-J, and Schwaiger M. Ga-68-PSMA PET/MR with multimodality image analysis for primary prostate cancer. Abdom Imaging 2015;40:1769–71. [PubMed: 25412869]

[31]. Eiber M, Maurer T, Souvatzoglou M, Beer AJ, Ruffani A, Haller B, et al. Evaluation of hybrid ^{68}Ga-PSMA ligand PET/CT in 248 patients with biochemical recurrence after radical prostatectomy. J Nucl Med. 2015;56:668–74. [PubMed: 25791990]

[32]. Malik N, Baur B, Winter G, Reske SN, Beer AJ, and Solbach C. Radiofluorination of PSMA-HBED via AlF Chelation and Biological Evaluations In Vitro. Mol Imaging Biol 2015.

[33]. Kung H New ^{68}Ga hbed-bisphosponates and their derivatives as bone imaging agents. J Nucl Med 2016;57:1106.

[34]. Alexoff D, Kim D, and Kung H. Radiopharmaceutical labeling device. United States Patent Application Publication No. US 2018/0250649 A1 2018 9 6.

[35]. Kolthammer JA, Su KH, Grover A, Narayanan M, Jordan DW, and Muzic RF. Performance evaluation of the Ingenuity TF PET/CT scanner with a focus on high count-rate conditions. Phys Med Biol 2014;59:3843–59. [PubMed: 24955921]

[36]. Protection ICoR. Basic Anatomical & Physiological Data for use in Radiological Protection - The Skeleton. ICRP publication 70, Table 47. Ann ICRP 1995;25:1–80.

[37]. Stabin MG, Sparks RB, and Crowe E. OLINDA/EXM: the second-generation personal computer software for internal dose assessment in nuclear medicine. J Nucl Med 2005;46:1023–7. [PubMed: 15937315]

[38]. Wahl RL, Jacene H, Kasamon Y, and Lodge MA. From RECIST to PERCIST: Evolving considerations for PET response criteria in solid tumors. J Nucl Med 2009;50:122S–50. [PubMed: 19403881]

[39]. Vanderhoek M, Perlman SB, and Jeraj R. Impact of the definition of peak standardized uptake value on quantification of treatment response. J Nucl Med 2012;53:4–11. [PubMed: 22213818]

[40]. Haynor DR and Woods SD. Resampling estimates of precision in emission tomography. IEEE Trans Med Imaging 1989;8:337–43. [PubMed: 18230533]

[41]. Dahlbom M Estimation of image noise in PET using the bootstrap method. IEEE Trans Nucl Sci 2002;49:2062–6.

[42]. Popescu LM, Matej S, and Lewitt RM. Iterative image reconstruction using geometrically ordered subsets with list-mode data. IEEE Nuclear Science Symposium and Medical Imaging Conference Piscataway, NJ; 2004, p. 3536–40.

[43]. Lim R, Fahey FH, Drubach LA, Connolly LP, and Treves ST. Early experience with fluorine-18 sodium fluoride bone PET in young patients with back pain. J Pediatr Orthop 2007;27:277–82 (Table 2). [PubMed: 17414009]

[44]. Bartel TB, Kuruva M, Gnanasegaran G, Beheshti M, Cohen EJ, Weissman AF, et al. SNMMI Procedure Standard for Bone Scintigraphy 4.0. J Nucl Med Technol 2018;46:398–404. [PubMed: 30518604]

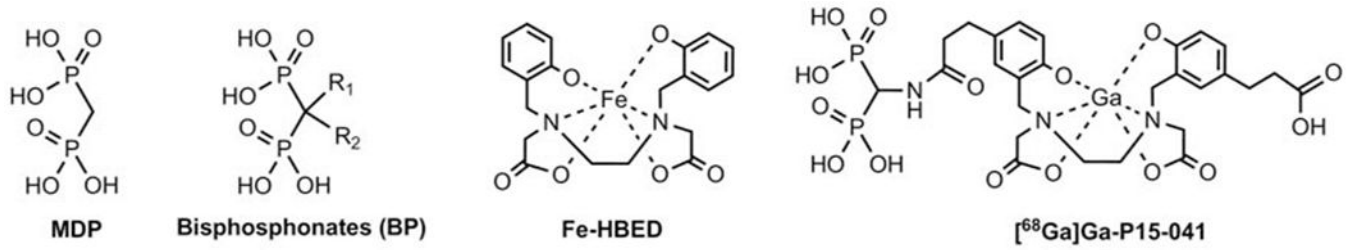

Fig. 1.

Chemical structures of methylene diphosphonate (MDP), bisphosphonates (BP), Fe-HBED, and [^{68}Ga]Ga-P15-041.

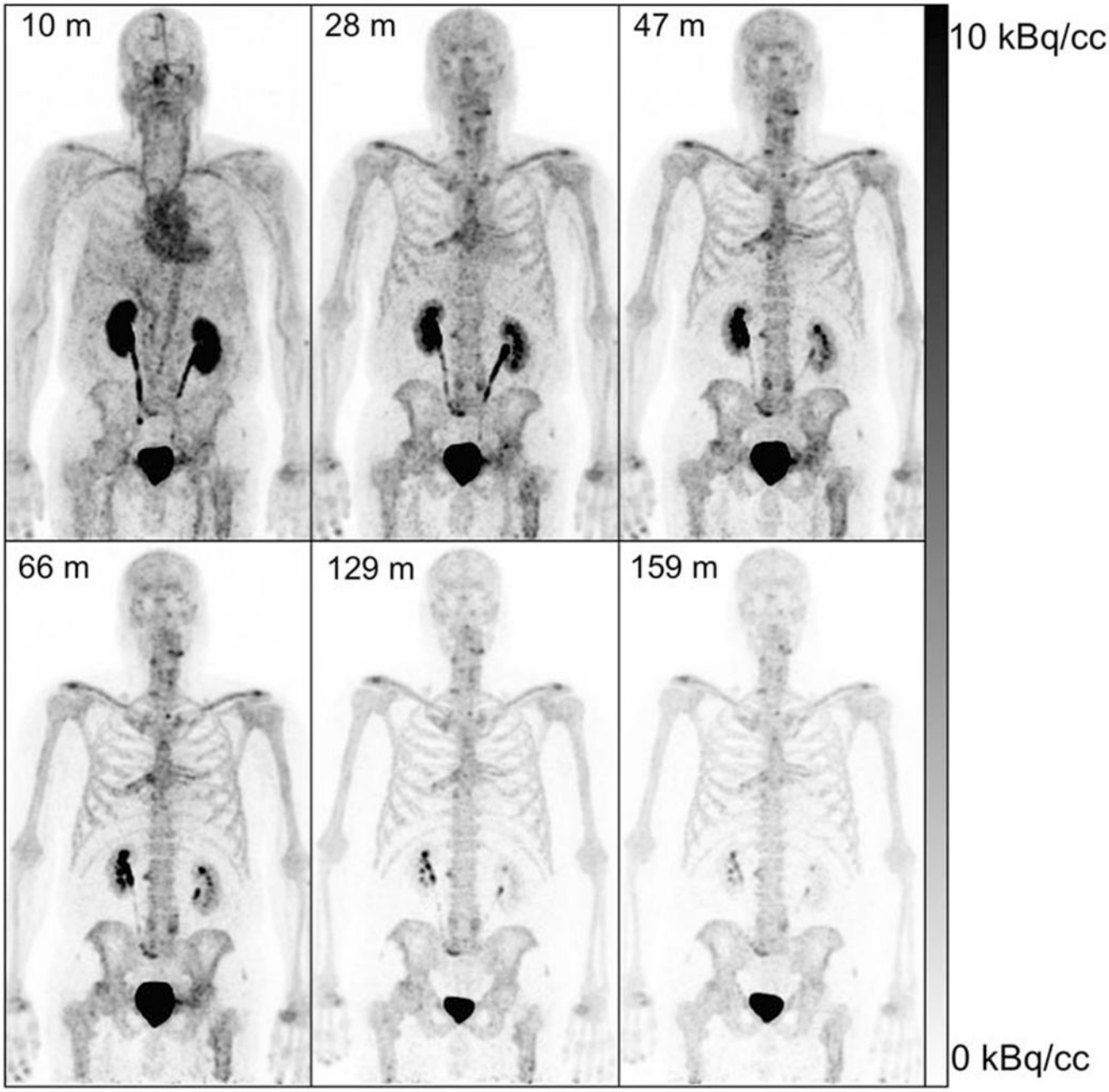

Fig. 2:

Maximum-intensity projections of [^{68}Ga]Ga-P15-041 of dosimetry subject 3 with scan midpoint times from tracer administration in minutes indicated in upper left using an injected activity of 232.2 MBq (6.28 mCi) and whole body images created as a composite of 90s scans in 10 bed positions for 15 minutes total. Images are scaled from 0 to 10 kBq/cc and decay corrected to the start time of each scan.

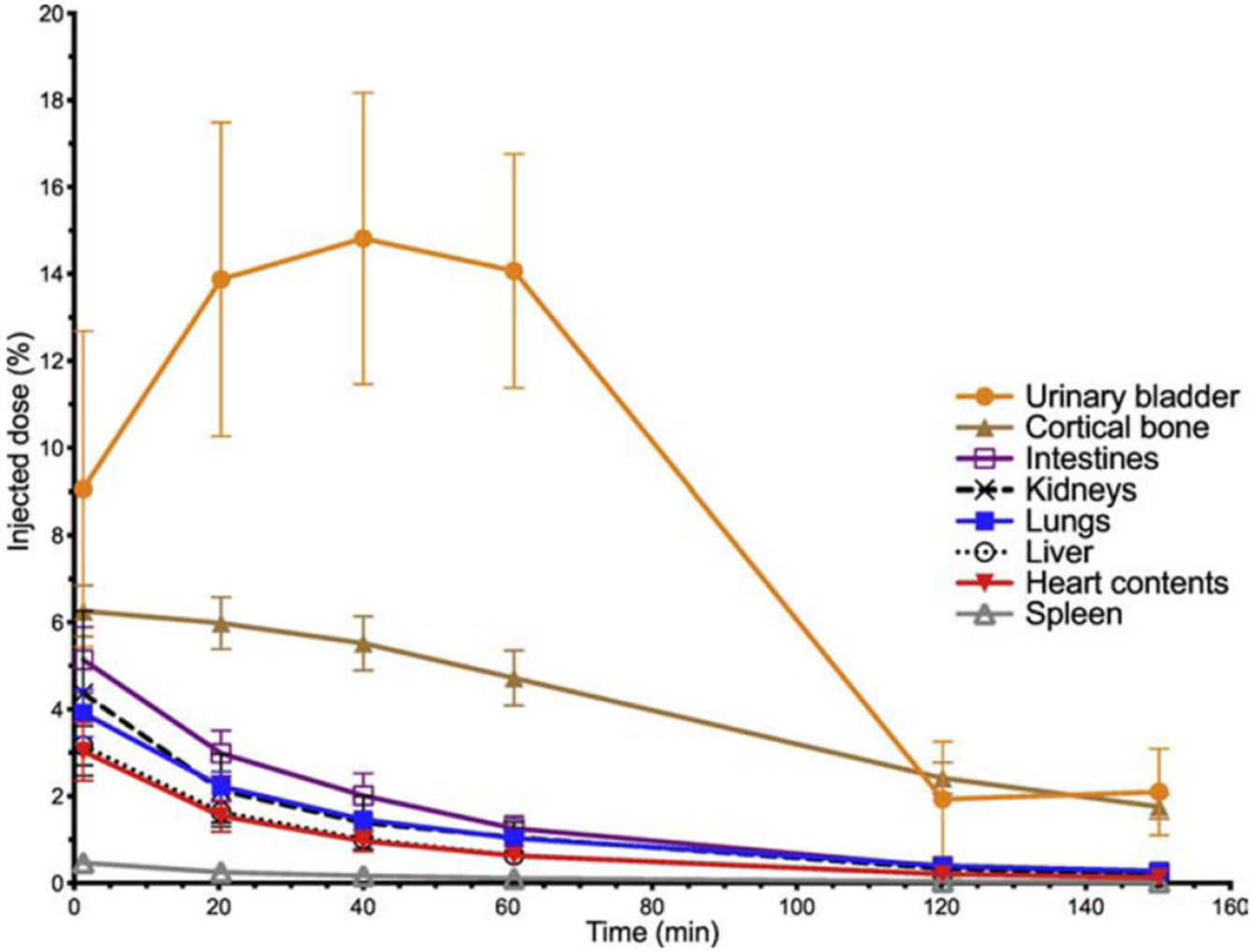

Fig. 3:

Mean [^{68}Ga]Ga-P15-041 injected activity percentages in organs as a function of time (± standard deviation bars, n = 8)

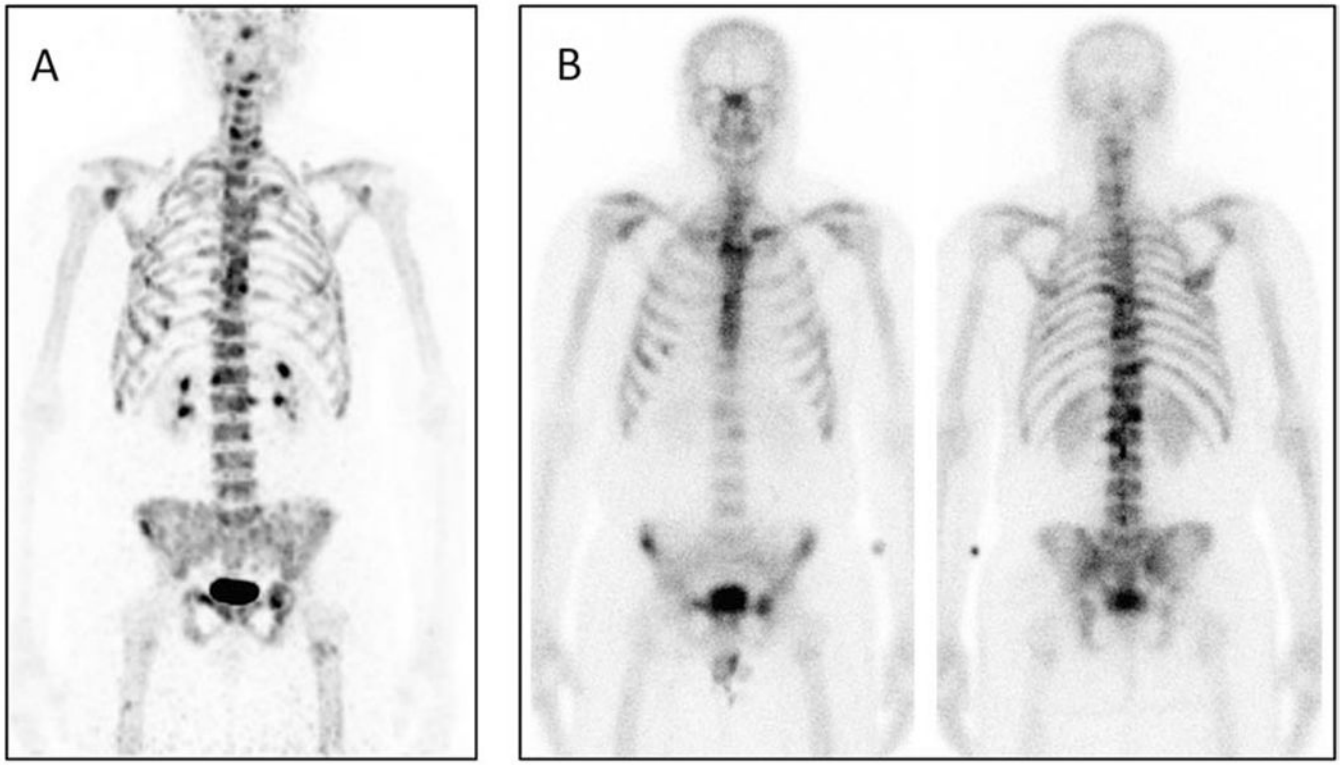

Fig. 4:

[A] Maximum-intensity projection (MIP) of [^{68}Ga]Ga-P15-041 uptake by dynamic cohort patient 2 with metastases in multiple ribs, vertebral bodies, pelvis, left clavicle, and right scapula. [B] Corresponding anterior and posterior views of [^{99m}Tc]Tc-MDP planar bone scintigraphy of same patient. The [^{68}Ga]Ga-P15-041 MIP was acquired from a decay corrected 15-minute whole body scan starting at 180 minutes post-injection of 193 MBq (5.22 mCi) and scaled from 0 to 15 g/mL SUV. The bone scan was acquired 22 days prior to the PET image for 24 min starting approximately 3 hours post-injection of 1080 MBq (29.1 mCi) of [^{99m}Tc]Tc-MDP.

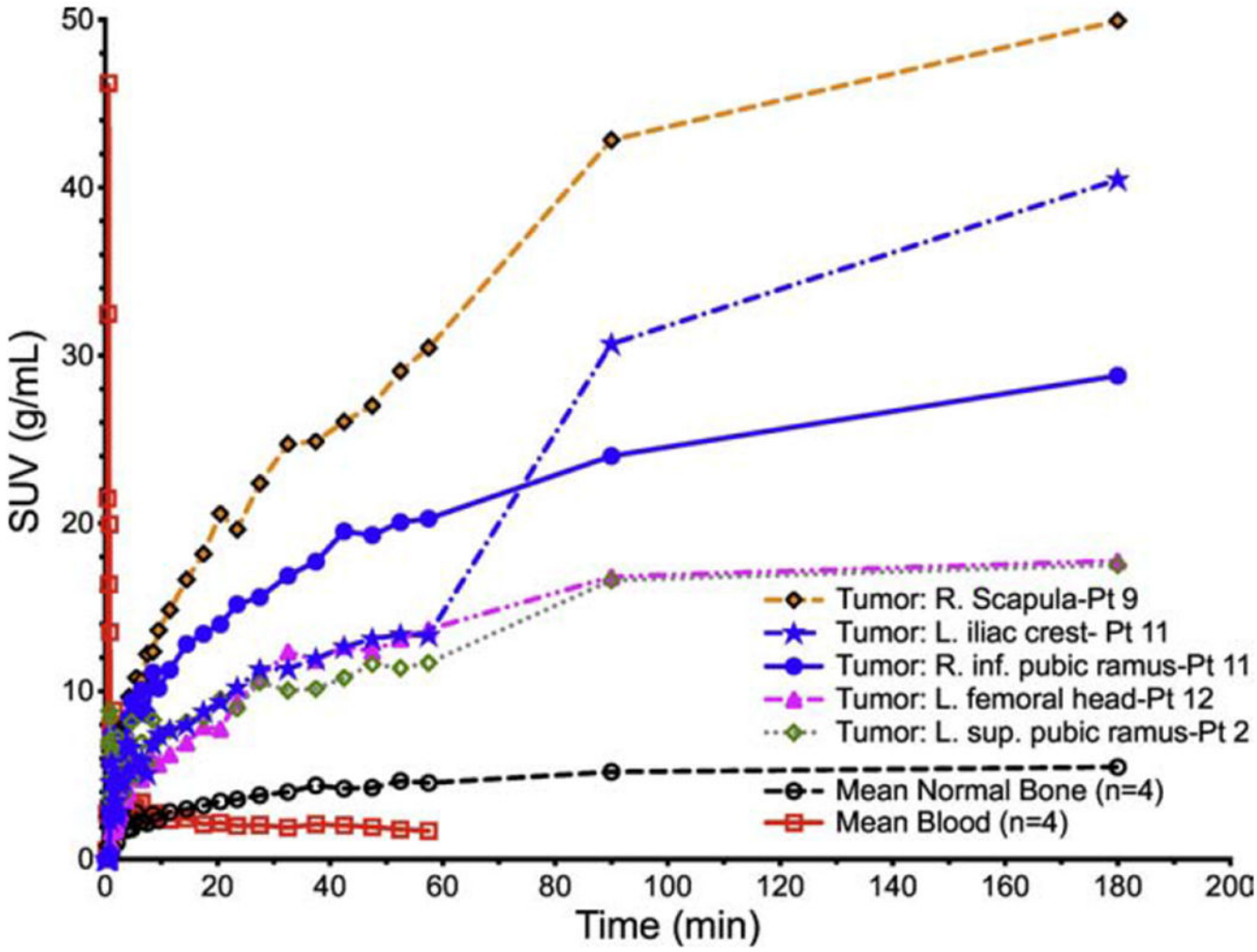

Fig. 5:

Peak standardized uptake values (SUV_P) for high [^{68}Ga]Ga-P15-041 uptake tumors from four volunteers with prostate cancer osseous metastatic disease, mean blood SUVs (n=4), and average normal bone (n=4) as a function of time.

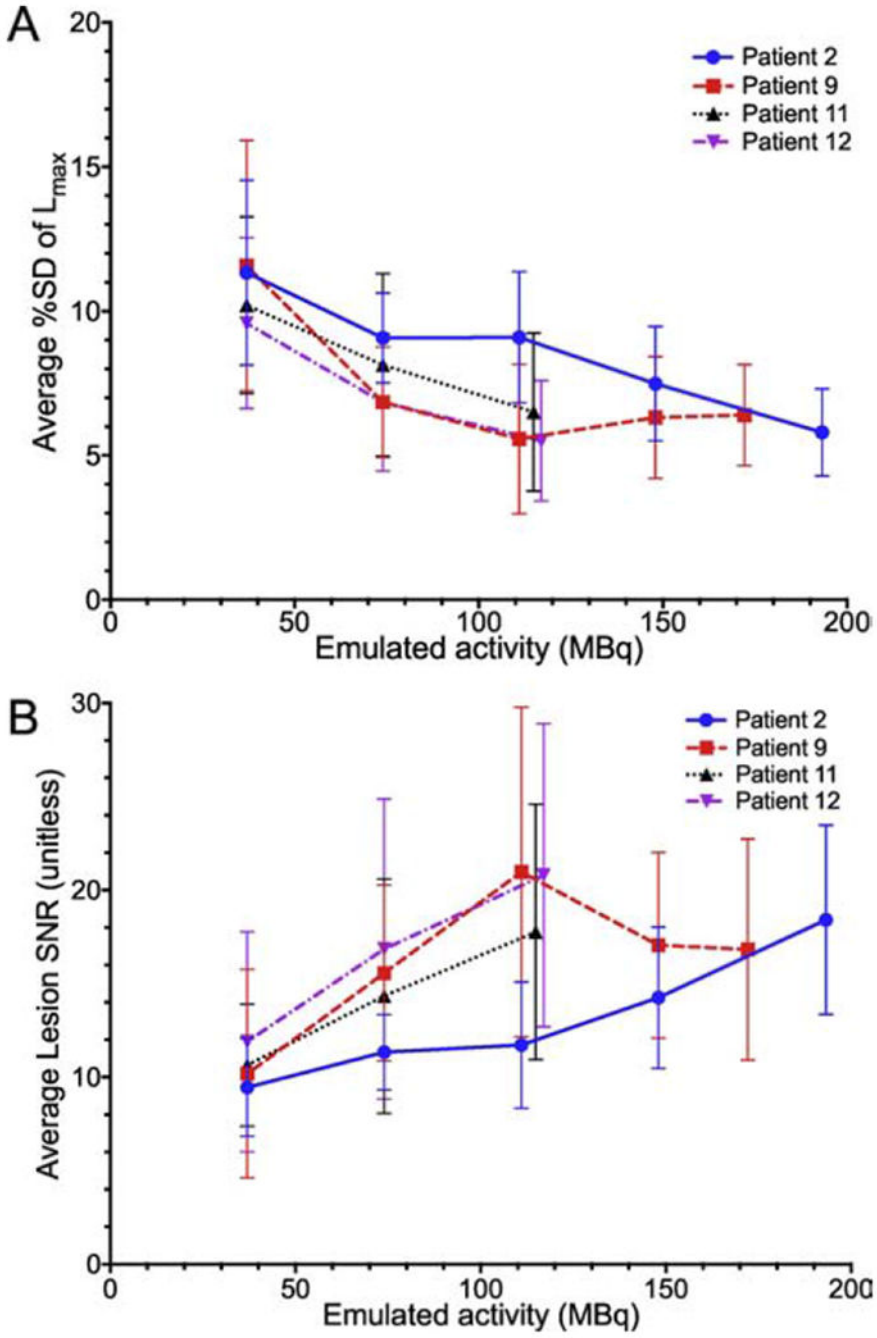

Fig. 6:

[A] Four volunteers' average variability of lesion max uptake (L_{max}) as a function of emulated injected activity. Each curve represents percentage standard deviation (%SD) across 10 bootstrapped replicates, averaged over all lesions in a single subject. The result for the injected activity is the rightmost point on each curve. Error bars are the ±SD over the lesions in a subject. [B] Lesion signal to noise ratio (L_{max} divided by %SD) calculated across each lesion.

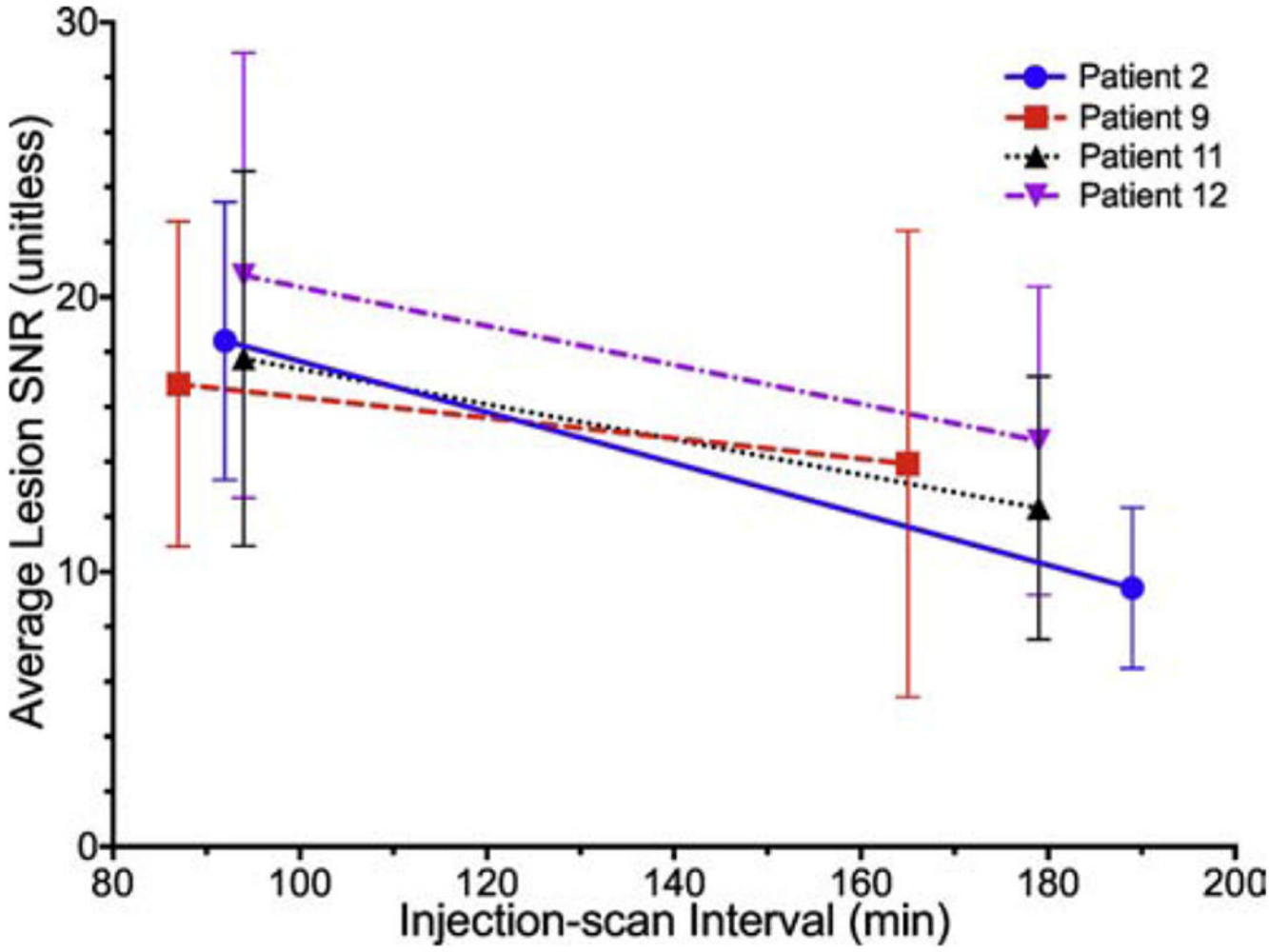

Fig. 7:
Four volunteers' average lesion signal-to-noise ratio (SNR) as a function of injection to scan start interval (min).

Table 1:

Subject demographic data

Patient	Age (y)	Height (cm)	Weight (kg)	Injected activity (MBq)	PSA level (ng/mL)	Gleason score	Cohort
1	59	180	85	194.8	1.94	8-9	Dosimetry
2	55	175	92.1	193.2	9.91	9	Dynamic
3	73	179	92.7	232.2	0.54	8	Dosimetry
4	66	169	111.1	204	0.68	7	Dosimetry
5*	63	174	109.4	187	17.94	9	Dynamic
6	71	179	98.7	146.8	1.02	5	Dosimetry
7	72	185	102	152.6	0.14	9	Dosimetry
8	63	175	100.9	145.7	4.95	7	Dosimetry
9	77	182	88	172.2	3.87	-	Dynamic
10	70	173	75.9	85.5	3.47	9	Dosimetry
11	69	162	84	114.9	90.83	9	Dynamic
12	76	187	78.9	117	5.01	-	Dynamic
13	69	178	89.9	158.7	<0.05	7	Dosimetry
Dosimetry mean (n=8)	68	177	94.5	165	1.82	7.4	
Dynamic mean (n=4)	69	177	85.8	149.3	50.37	9**	

*Subject 5 was excluded from analyses due to early end of PET scan (after 27 min).

**Gleason score for dynamic cohort limited to n=2

Table 2:

[^{68}Ga]Ga-P15-041 absorbed dose estimates in mSv/MBq for 8 male humans

Target organ	Mean	Standard deviation
Adrenals	1.02E-02	8.19E-04
Brain	3.57E-03	8.38E-04
Breasts	8.07E-03	6.32E-04
Gallbladder wall	1.03E-02	8.15E-04
Lower large intestine wall	1.29E-02	8.65E-04
Small intestine	2.41E-02	3.59E-03
Stomach wall	9.77E-03	7.54E-04
Upper large intestine wall	1.97E-02	2.68E-03
Heart Wall	1.98E-02	2.93E-03
Kidneys	4.93E-02	1.70E-02
Liver	8.16E-03	1.23E-03
Lungs	1.73E-02	2.53E-03
Muscle	9.19E-03	5.43E-04
Ovaries	1.16E-02	5.91E-04
Pancreas	1.03E-02	8.15E-04
Red Marrow	8.04E-03	4.87E-04
Osteogenic cells	2.63E-02	1.93E-03
Skin	7.85E-03	5.55E-04
Spleen	1.17E-02	1.68E-03
Testes	9.57E-03	3.90E-04
Thymus	9.26E-03	7.05E-04
Thyroid	8.92E-03	7.06E-04
Urinary bladder wall	1.35E-01	7.59E-02
Uterus	1.33E-02	1.35E-03
Total Body	1.07E-02	6.33E-04
Effective dose equivalent	2.31E-02	4.59E-03
Effective dose	1.73E-02	3.64E-03